Interactions between MC3T3-E1 cells and textured Ti6Al4V surfaces

W. O. Soboyejo,[1,2] B. Nemetski,[1,2] S. Allameh,[1,2] N. Marcantonio,[3] C. Mercer,[1,2] J. Ricci[4]
[1]*Princeton Materials Institute, Princeton University, Princeton, New Jersey 08544*
[2]*The Department of Mechanical and Aerospace Engineering, Princeton University, Princeton, New Jersey 08544*
[3]*Division of Engineering, Brown University, Providence, Rhode Island 02912*
[4]*Department of Prosthodontics, University of Medicine and Dentistry of New Jersey, Newark, New Jersey 07103*

Received 20 July 2001; revised 8 November 2001; accepted 11 January 2002

Abstract: This paper presents the results of an experimental study of the interactions between MC3T3-E1 (mouse calvarian) cells and textured Ti6Al4V surfaces, including surfaces produced by laser microgrooving; blasting with alumina particles; and polishing. The multiscale interactions between MC3T3-E1 cells and these textured surfaces are studied using a combination of optical scanning transmission electron microscopy and atomic force microscopy. The potential cytotoxic effects of microchemistry on cell–surface interactions also are considered in studies of cell spreading and orientation over 9-day periods. These studies show that cells on microgrooved Ti6Al4V geometries that are 8 or 12 μm deep undergo contact guidance and limited cell spreading. Similar contact guidance is observed on the surfaces of diamond-polished surfaces on which nanoscale grooves are formed due to the scratching that occurs during polishing. In contrast, random cell orientations are observed on alumina-blasted Ti6Al4V surfaces. The possible effects of surface topography are discussed for scar-tissue formation and improved cell–surface integration. © 2002 Wiley Periodicals, Inc. J Biomed Mater Res 62: 56–72, 2002

Key words: cell–surface interactions; MC3T3-E1 cells; Ti6Al4V; surface textures; laser microgrooves

INTRODUCTION

In recent years, the Ti6Al4V alloy has been used extensively in biomedical applications such as hip replacements[1,2] and dental implants[3,4] due largely to its attractive combinations of mechanical properties,[1,2] corrosion resistance,[2] and biocompatibility.[1–4] In most applications, the integration of Ti6Al4V with bone cells is the key to a successful integration of the implant.[1] For example, in the case of Ti6Al4V hip implants, the interface between bone cement and Ti6Al4V can be degraded by the osteolysis that occurs as a result of interactions with polyethylene particles that are liberated due to contact between the polyethylene cap and Co-Cr/Co-Cr-Mo or ceramic (ZrO_2 or Al_2O_3) heads that are used in modern hip implants.[5,6] Since the subsequent detachment/delamination of the stem from the femur may result in patient discomfort and the need for implant retrieval/replacement within 10–15 years,[1–4] there is a need to explore various means of improving the integration of bone cells with Ti6Al4V surfaces.

One method used to improve bone cell–Ti6Al4V integration involves the use of roughened surfaces produced by blasting surfaces with alumina or silica particles.[3,7] Such roughened surfaces appear to promote cell–surface attachment while limiting the extent of cell spreading. However, blasted surfaces also have complex microchemistries, and they may contain higher levels of cytotoxic elements such as Al or V.[7] Blasted surfaces also may give rise to random cell orientations that may give rise to scar tissue formation.[8]

The other approach that is being explored for the design of improved cell–surface integration involves the use of microgrooved Ti6Al4V geometries.[3,4,9–13] Such microgroove geometries can be produced by laser texturing[3,4] or by microfabrication processes.[9–11] In the case of Ti6Al4V, laser microgrooves with dimensions (depths) between ~1–16 μm have been produced. Such grooves have been shown to result in improved adhesion/integration in animal (dog) implant studies.[4] They also have been shown to reduce the extent of scar tissue formation, due possibly to the alignment of cells via contact guidance.[8] However, al-

Correspondence to: W. Soboyejo; e-mail: soboyejo@princeton.edu

Contract grant support: Princeton University (start-up funds provided to WOS)

© 2002 Wiley Periodicals, Inc.

though the occurrence of contact guidance has been demonstrated on standard microgrooved polystyrene culture plates,[3,8] we are unaware of any prior demonstration of contact guidance on laser-textured Ti6Al4V surfaces.

This paper presents the results of an experimental study of bone cell (MC3T3-E1) /Ti6Al4V surface interactions. The surfaces that are studied include a polished control surface; an alumina-blasted surface, and two laser microgrooved surfaces with depths of 8 and 12 μm. Following the description of the initial material and surface texturing schemes, the hierarchies of surface topography and microstructural/substructural features that can contribute to cell–surface integration are considered at multiple-length scales between nano- and microscale. This is achieved by describing images obtained using atomic force microscopy (1–5 nm resolution); transmission electron microscopy (5–10 nm resolution); scanning electron microscopy (10 nm-microscale). Changes in the surface and near-surface microchemistry then are discussed and the results of 9-day cell-culture studies are presented. Finally, the implications of the current results are examined.

MATERIALS AND METHODS

Material and surface-texturing schemes

A canine intramedullary rod model was used to study the effects of surface texture (Fig. 1). The textured surfaces were produced from forged α/β Ti6Al4V. The forged Ti6Al4V material was obtained from three sources: (1) Laser-textured surfaces were supplied by Resonetics, Nashua, NH. These materials had grooves that were either 8 or 12 microns in diameter. The groove dimensions were selected to be in a size range comparable to the selected bone-cell sizes (average size, ~10 μm). The laser grooves were engraved into the surfaces of cylinders that were approximately 6.5 mm in diameter and about 9 mm long. The grooves were made using a pulsed, computer-controlled Excimer laser system and large-area masking techniques.[3,4] The laser grooves were patterned by controlled sample motion in the longitudinal and circumferential directions. Thus the grooves were aligned along longitudinal and transverse orientations.

(2) Blast-textured surfaces also were obtained from Howmedica Osteonics of East Rutherford, NJ. These were produced by blast texturing with alumina pellets. (3) And finally, mechanically polished surfaces were studied as a control. These were obtained at The University of Medicine and Dentistry of New Jersey (UMDNJ) by polishing surfaces sequentially on a cloth wheel with different grit sizes. Low magnification mesoscale scanning electron microscopy images of the textured surfaces are shown in Figure 1. The associated surface topographies and microstructural features will be discussed later.

Surface topography and microstructure

Since the interactions between bone cells and Ti6Al4V surfaces can occur at multiple-length scales between the nano- and microscale, it is of interest to characterize surface topography and microstructural/substructural features with a range of techniques that facilitate imaging across multiple-length scales. At the nanoscale, atomic force microscopy (AFM) was used to characterize surface topography. Between the nano- and microscale, scanning and transmission electron microscopy were used to study substructural and microstructural features that can contribute to cell–surface interactions.

Cell culture experiments

In an effort to develop a basic understanding of the initial stages of cell–surface integration, cell culture experiments were carried out with MC3T3-E1 (mouse calvarian) cells/osteoblasts. These have been shown to exhibit phenotypes that are similar to those expressed by human osteoblasts.[12] The 9-day cell culture experiments were performed on polished control surfaces, alumina-blasted surfaces, and 8- and 12-μm laser microgrooved surfaces. Details of the experimental methods are given below.

Cell culture

MC3T3-E1 mouse osteoblast cells were maintained at 37°C in humid 5%CO_2–95% air. The culture medium was 89% DMEM, 10% fetal bovine serum, and 1% penicillin/streptomycin. The cells were split 1:5 whenever confluence was reached (which occurred after 5–7 days). The cells were harvested using trypsin at 0.25% concentration; the cells then were centrifuged down to a pellet at 3500 revolutions per min (RPM) and resuspended in 1 mL of medium.

Ti6Al4V surfaces

Longitudinal slices were taken from hollow cylindrical sections that had been extracted from canine intramedullary rods [Fig. 1(b,c)]. These were each cut circumferentially into several smaller sections, giving four basic surfaces: 12-μm grooves, 8-μm groves, alumina-blasted, and a smooth control surface. Prior to seeding the cells, the surfaces were cleaned and passivated. First the surfaces were sonicated for 15 min in acetone, then for 15 min in detergent, after which each section individually was rinsed in distilled, deionized, autoclaved H_2O (ddH_2O) 4–5 times. Each surface then was passivated in 15% nitric acid for 30 min and rinsed 4–5 times in ddH_2>0. They then were stored in 70% EtOH until use. Before use they again were rinsed 4–5 times in ddH_2O and dried in a clean hood.

Preparation for SEM analysis

The surfaces were removed from the media at 1-, 2-, 5-, and 9-day intervals. To remove detritus, they were rinsed in

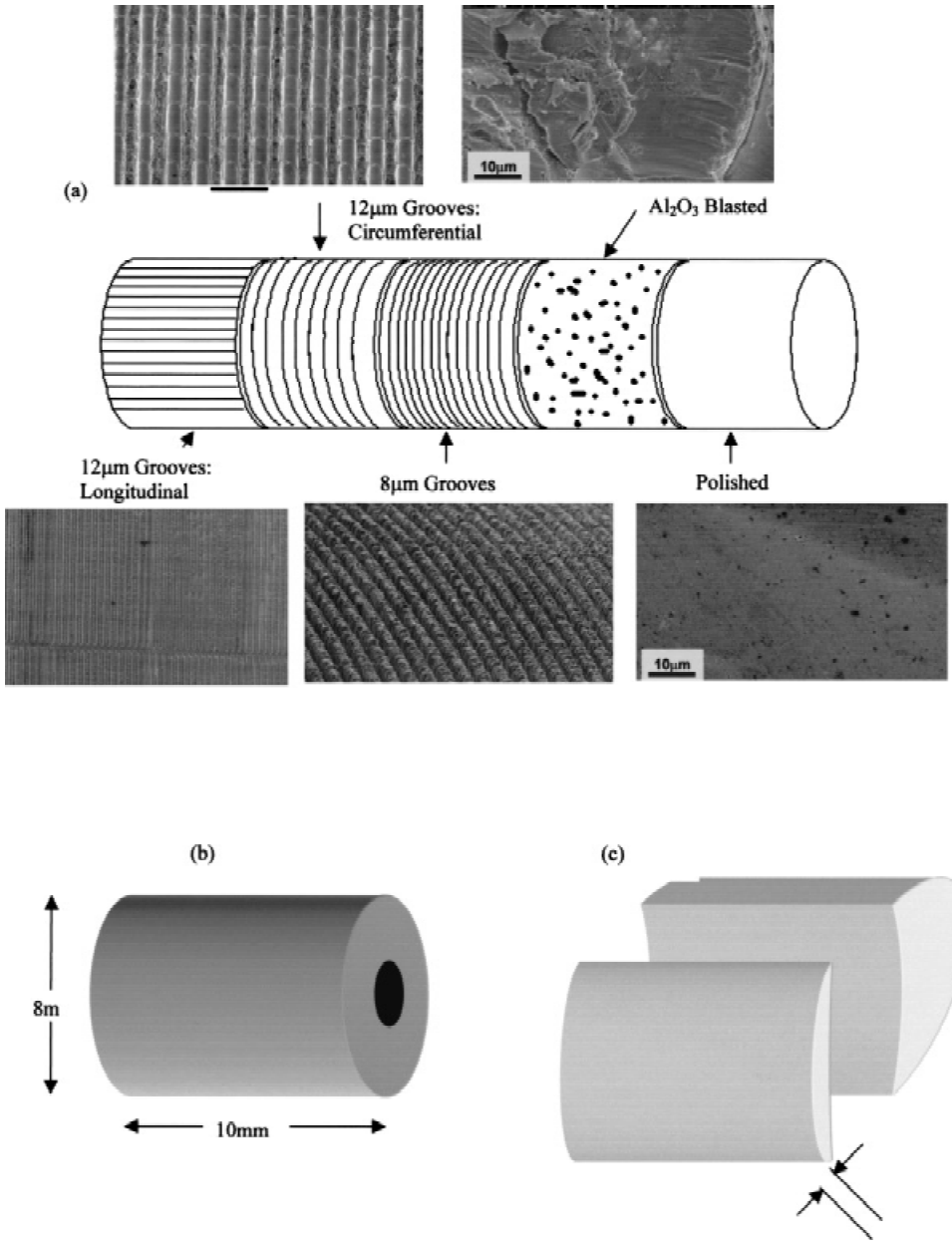

Figure 1. Overview of (a) intramedullary rod and SEM images of textured surfaces; (b) cylindrical 0.8-m disk; and (c) longitudinal cross section.

0.1*M* of sodium phosphate buffer at 7.4 pH and fixed overnight in 0.1*M* of sodium phosphate buffer with 3% glutaraldehyde. The surfaces were removed from the 3% glutaraldehyde and stored in 0.1*M* of sodium phosphate buffer until they were ready for dehydration. The cells were dehydrated via a stepwise (30 min each step) alcohol dehydration (30, 50, 70, 80, 90%, and 3 × 100%).

The cells then underwent a critical point drying in CO_2, and to remove the ethanol the chamber was flushed 5–6 times at 15-min intervals. The surfaces were fixed by epoxy to SEM stubs and sputter-coated with a gold–palladium (Au-Pd) alloy. The latter was done to create conducting surfaces for subsequent scanning electron microscopy (SEM) analysis.

RESULTS AND DISCUSSION

Nanoscale characterization of surface topography

In the current study, multiscale characterization revealed a number of features that may be important for the optimization of surface-texturing schemes. At the nanoscale, surface topographies were characterized using atomic force microscopy (AFM). The current study shows clearly that mechanical polishing can be used to introduce grooves at the nanoscale [Fig. 1(a)]. Furthermore, Al_2O_3-blasted surfaces have channels

[Fig. 1(b)] that are associated with the direction of incidence of the alumina particles. The channel characteristics, therefore, may be varied by controlling the incidence angles, velocities, and sizes of the incoming particles.

Similarly, the surface roughness levels in the laser-textured surfaces are clearly in the nanoscale regime [Fig. 2(c,d)]. At this scale, the laser-textured surfaces have a much higher surface roughness than do the Al_2O_3-blasted and polished surfaces (Table I). This may contribute, at least partly, to the improved adhesion of laser-textured Ti6Al4V surfaces to tissue.[3,4] However, further research is needed to explore the contributions of nanoscale surface topography of Ti6Al4V to cell and tissue adhesion.

Due to the complex nature of surface topographies, it is difficult to utilize a single roughness parameter in a complete characterization of surface topography. One possible approach is to separate the roughnesses into several windows, such as the wavelength-dependent roughness approach of Wieland et al.[13] The roughness also may be characterized by a less accurate characteristic roughness parameter, such as a root mean-square roughness (RMS) value or a fractal number[14,15] (Table I). These provide single numbers that may be used for comparisons of roughness. However, they do not provide complete descriptions of the local details of the surface topographies.

TABLE I
Summary of AFM Surface Roughness and Fractal Dimension Measurements

Type of Surface	RMS Roughness (nm)	Fractal Dimension
12-μm grooves	117 ± 26	2.06 ± 0.017
8-μm grooves	71 ± 15	2.07 ± 0.019
Al_2O_3-blasted	44 ± 16	2.09 ± 0.037
Polished	32 ± 5	2.10 ± 0.012

In this study, characteristic fractal and RMS measurements of surface roughness, obtained via AFM, were used for the comparisons of surface roughness. It is important to note that surface roughness decreases

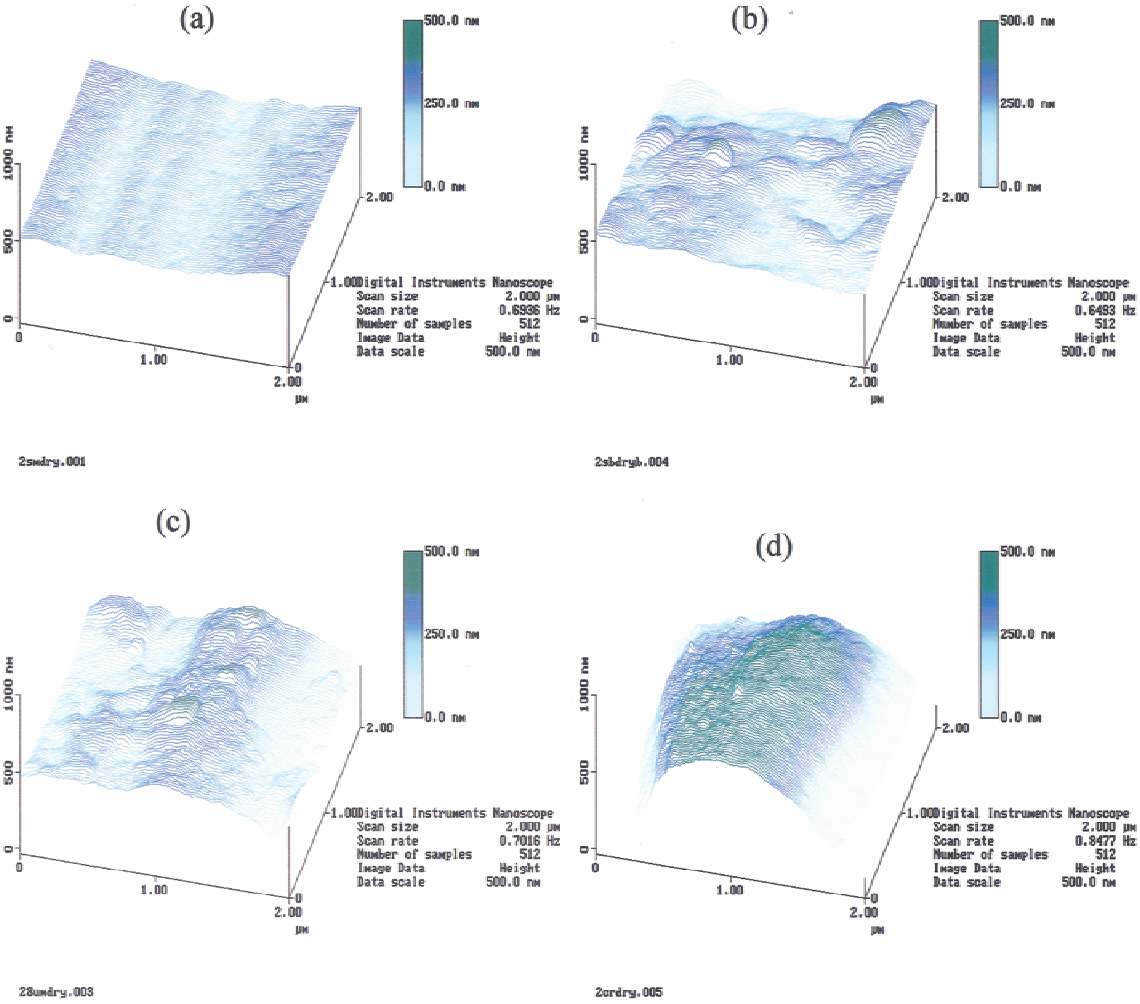

Figure 2. Tapping AFM images. (a) Polished surface; (b) alumina-blasted surface; (c) 8 μm deep groove geometry; and (d) 12μ deep groove gemometry. [Color figure can be viewed in the online issue, which is available at www.interscience.wiley.com.]

with increasing fractal numbers. Also, surface roughness increases with increasing RMS roughness. In any case, both measures of surface roughness may be used in quality control and standardization of commercial surface texturing schemes at the nanoscale.

However, accurate descriptions of surface topography should employ the wavelength-dependent approaches of Wieland et al.[13] Furthermore, the differences in the fractal numbers (associated with different surface textures) are relatively small compared to the differences in RMS roughness values (Table I). The RMS roughness values show that the Excimer laser-grooved surfaces are rougher than the alumina-blasted surfaces, which, in turn, are rougher than the polished surfaces. Furthermore, the fractal numbers show that the geometric complexity of the surface is affected less by surface processing, as opposed to the RMS, which is affected more by surface processing.

Submicron characterization of microstructure

At the submicron scale (between nano- and micron scale), transmission electron microscopy (TEM) analysis of the laser-textured Ti6Al4V material revealed a microstructure that is similar to that of laser-welded α/β titanium structures (Figs. 3 and 4).[5] This includes a complex layered solidification microstructure, consisting primarily of α-phase. This latter is somewhat surprising in view of the expected depletion of aluminum (an α-stabilizer with a much lower melting point than Ti or V) in the surface regions near the laser-induced melt pool. In any case, the TEM analysis revealed predominantly α structures at the bottom and the top of the grooved structures (Figs. 3 and 4).

Energy dispersive X-ray spectroscopy (EDS) analysis of the bottom of the grooves also indicated some contamination by Mo, Cr, and other elements, which may affect the performance of laser-grooved structures. The source of these elements is yet to be established. Nevertheless, it is likely that they were incorporated into the grooved structures during laser ablation. Some control of the laser processing equipment and environment therefore is recommended to identify the source of the contaminants, which may give rise to the increased stabilization of the β phase. Post-processing heat treatment also may be used to homogenize the microstructures and phase compositions.

Micro- and mesoscale characterization of microstructure

Optical microscopy (OM) and scanning electron microscopy (SEM) were used to study the microstructural features with sizes between the micro- and mesoscale. The microstructural features were somewhat reminiscent of those reported in earlier work on titanium alloys.[16–19] In the case of the smooth, polished surfaces, uniform microstructures were observed across the cross sections [Fig. 5(a)]. These consisted of twinned equiaxed α/β grains reminiscent of mill-annealed Ti6Al4V after forging in the α/β phase field.[17]

The high incidence of deformation-induced twinning is due to the significant amount of plastic work that was done during hot working. Twinning is a common deformation made in the hexagonal close-packed structure of the α–phase, which is known to have only four independent slip systems.[18] Since homogenous plastic deformation requires the operation of five independent slip systems,[18,19] the occurrence of deformation-induced twinning provides an alternative means of accommodating shape change without inducing grain boundary incompatibility or microcracking.

At the microscale, optical microscopy (OM) and scanning electron microscopy (SEM) analyses reveal a complex re-solidification microstructure in the laser-textured surfaces. This includes re-solidified sections that had been melted by the laser beam and the associated heat-affected zones [Fig. 5(a–f)]. The structures therefore are somewhat analogous to those of laser-welded α/β-titanium alloys.[16]

The higher magnification imaging of the SEM revealed that cracks are present in the re-solidified zone after laser processing [Fig. 5(c)]. Since these cracks may grow during subsequent fatigue loading in biomedical applications such as hip or dental implants,[1–4] it is important to eliminate them by controlling the laser processing parameters. Post-weld heat treatment also may be used to control the microstructural features that are present in the textured surfaces following laser processing.[16]

The mesoscale is the regime between the micro- and macro-regimes. It corresponds to clusters of cells (tissue) or clusters of grains that can interact with each other. This interaction is critical in the adhesion of tissue to bone cells.[3,4,9–11,20–25] This has been shown in prior studies of cell interaction with textured tissue culture plates[3,4] and Ti or Ti6Al4V surfaces.[9–11,20–25]

There also have been some prior studies of cell–surface interactions between rat dermal fibroblasts (RDF) and smooth or microgrooved (1–10 μm wide and 0.5 μm deep) geometries in polystyrene (PS),[3,4] fibroblasts and polystyrene,[26–28] silicone,[29] and a range of other surfaces.[30–43]

All the above studies show that cells respond to groove geometry and surface topography, although cell response is cell-type dependent. However, there is no general consensus on the effects of microgroove dimensions. It also is unclear whether cell attachment

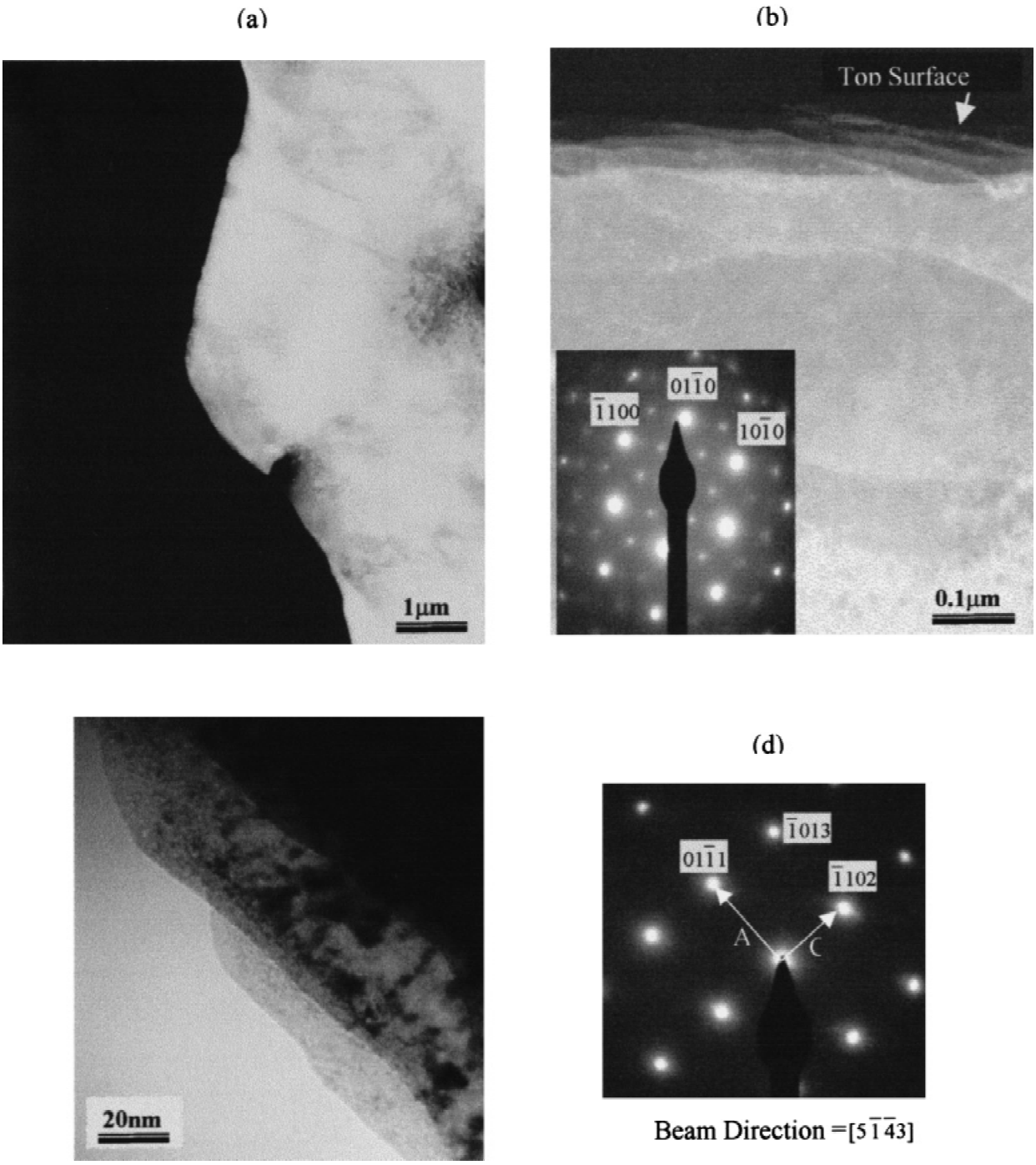

Figure 3. Bright-field images from the top of the ridges on the laser-grooved sample together with corresponding diffraction patterns. (a) Low-magnification bright-field image showing both top and bottom of a groove; (b) layered structure (shown with an arrow) of the top of the ridge together with a diffraction pattern insert; (c) high-magnification BF image of the layered structure of the flank of the groove; and (d) the corresponding diffraction pattern of the flank of the groove with main reflections indexed. The beam directions of diffraction patterns are 0001 and 5143, respectively.

or proliferation will occur for a given groove configuration.

Nevertheless, it is important to examine the two types of cell response (attachment or proliferation) that have been reported to occur on microgrooved surfaces.[3,4,9–11,22–31] At one extreme, cells have been shown to attach and elongate without proliferation.[3,4] This appears to occur when the groove widths are comparable to the cell size. This results in cell attachment to the tops, bottoms, and sides of the grooves when the cell sizes are comparable to the groove width of 12 μm. The rat tendon fibroblast cells are aligned along the longitudinal axis of the microgrooves, showing classical evidence of contact guid-

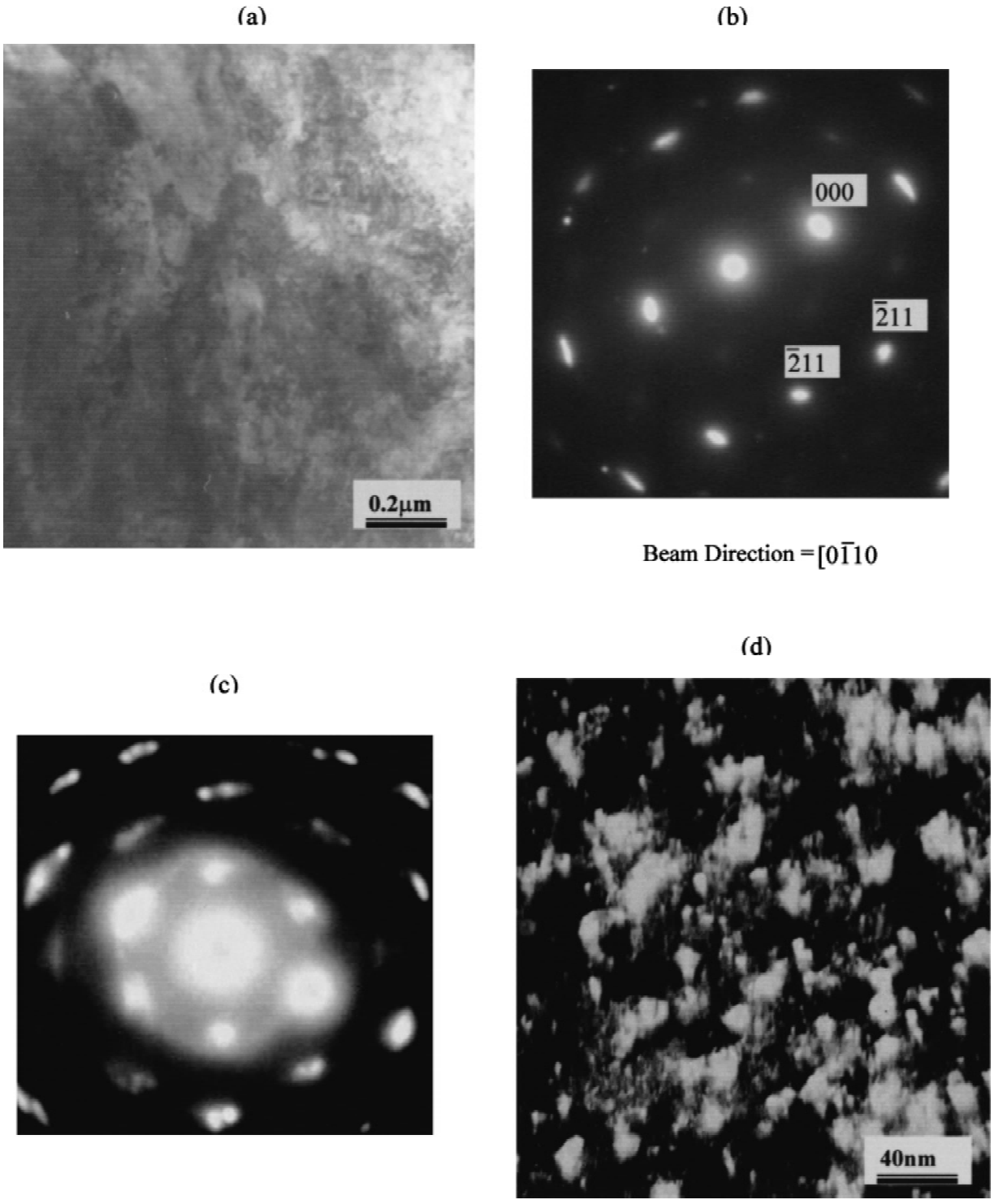

Figure 4. (a–d) Bright-field images from the tops of areas at the bottom of grooves and the sides of adjacent ridges, showing contrast due to second-phase particles and impurities. Corresponding diffraction patterns are shown in (b) diffraction pattern made with a [0110]-type beam; (c) diffraction pattern from the bottom of the groove showing extra spots caused by impurities and second-phase particles; and (d) DF image made from a reflection belonging to the corresponding reflection in the diffraction pattern of (c). The impurities and second-phase particles are illuminated in the dark-field image.

ance. In contrast, cells proliferate when the grooves (2 μm in width) are smaller than the cell sizes. The cells then span several grooves and still are aligned along the longitudinal axis of the grooves.[3,4]

The results presented in references 3 and 4 are somewhat different from those reported by Walboomers et al.[32] relative to the attachment of rat dermal fibroblasts (RDF). These studies on 1–10-μm wide

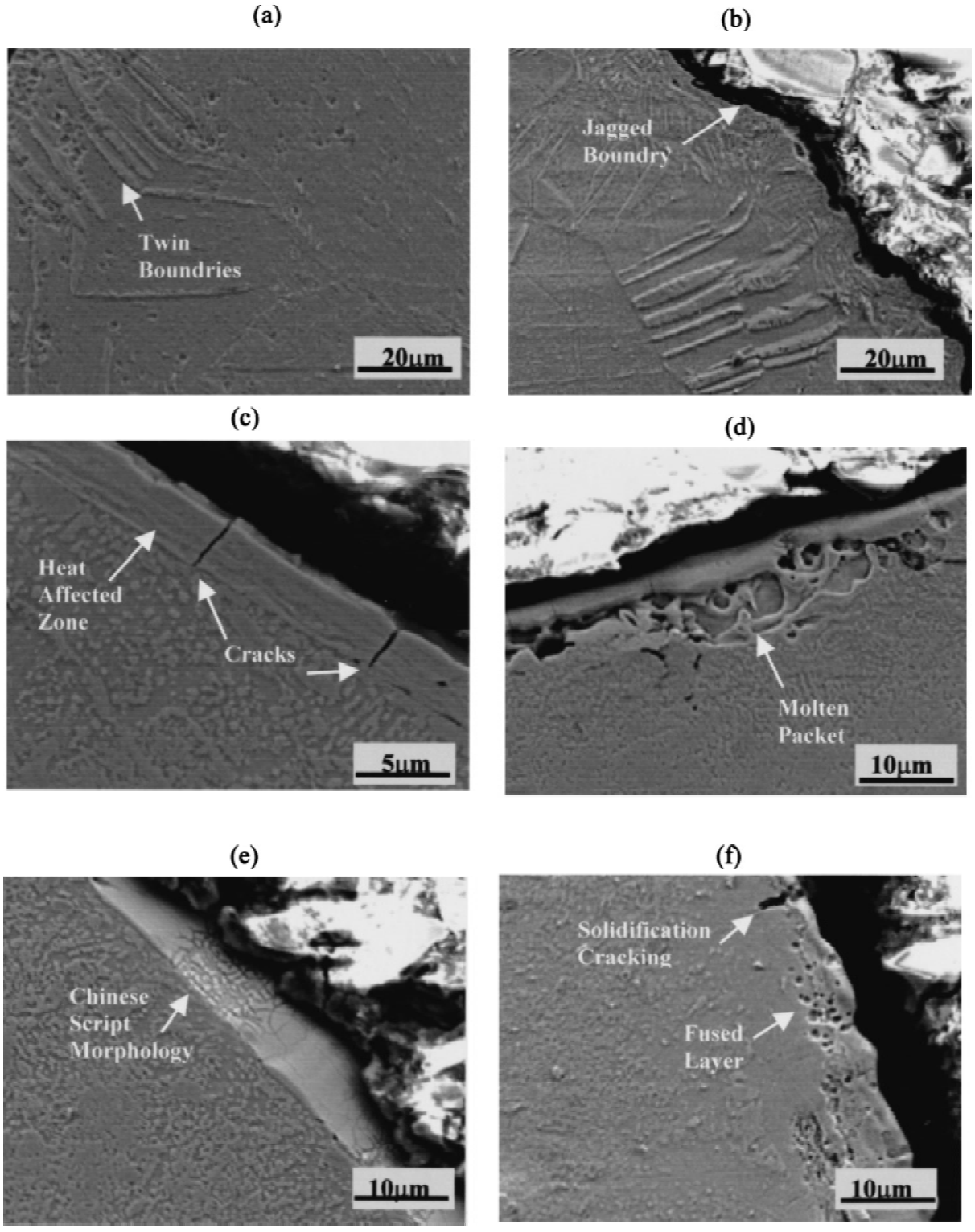

Figure 5. Scanning electron micrographs of Ti6Al4V specimens: (a) bulk material of polished specimen; (b) outer edge of grit-blasted specimen; (c) heat-affected zone, fused layer, and solidification cracking in 8-μm circumferentially grooved specimen; (e) heat-affected zone, fused layer, and solidification cracking in 12-μm circumferentially grooved specimen; and (f) heat-affected zone, fused layer, and solidification cracking in 12-μm longitudinally grooved specimen.

grooves show that RDF cells proliferate on all grooves with dimensions in this range. Similar responses also were observed on grooved polystyrene (PS) and pure titanium (Ti) substrates. The cells on the 1–2-μm wide grooves were reported to be better oriented than those on the 5–10-μm grooves. Cultured cells in the 1–2-μm grooves appeared to lie on top of the grooves while those in the 5–10-μm grooves descended more fre-

quently into the grooves. However, the cells cultured on pure Ti were less aligned with the grooves than were the cells cultured on PS.

Finally, it is important to note here that some recent work[33–36] suggests that surface micropatterning may be used to guide or control cell biochemical response. However, further work is clearly needed to establish the reasons for the observed contact guidance and cell proliferation phenomena. *In vitro* experiments[3] also are needed to provide an improved understanding of how the hierarchies of length scales (among the nano-, micro-, and mesoscales) contribute to the attachment/adhesion of cells and tissue to surface-textured biomedical materials such as Ti6Al4V.

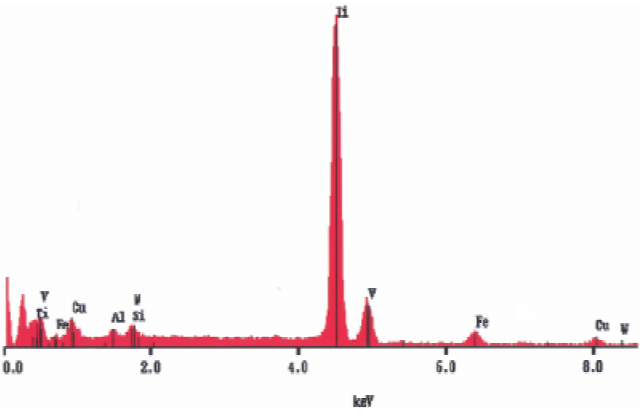

Figure 6. EDS spectrum of a typical grooved surface. Note the lack of a defined aluminum peak and the presence of impurities such as Fe. [Color figure can be viewed in the online issue, which is available at www.interscience.wiley.com.]

Microchemistry

The fabrication process itself can introduce a change in the surface composition. Both laser grooving and alumina blasting can affect the surface, by vaporization and embedding, respectively. Therefore energy dispersive X-ray spectroscopy (EDS) analysis was performed during scanning and transmission electron microscopy examination of the textured surfaces. The submicron microstructural/substructural features in a laser-grooved sample were examined in a transmission electron microscope operated at 200 keV. Figure 3(a) shows a low magnification bright-field image of the edge of a cross-sectional sample displaying a ridge and a valley. Energy dispersive X-ray spectroscopy (EDS) analysis was performed on the sample to further examine changes in the composition due to melting and re-solidifying of the material removed from the grooves and deposited on the adjacent ridges.

Initial inspection of the microstructure at the top of the ridges [Fig. 3(a)] shows a layered structure [Fig. 3(b)]. This structure may be associated with multiple liquid transfers (after each laser pulse) from the bottom of adjacent grooves. No difference was observed in the diffraction patterns obtained from these layers, leading to the conclusion that they are solidified with similar orientations.

The EDS analysis of the layered region showed all the energy peaks corresponding to Ti and V. No substantial energy peaks were detected for aluminum, indicating a depletion of aluminum in this region (Fig. 6). Since the melting of Ti occurs at temperatures that are much greater than those of aluminum, some loss of aluminum is expected due to the evaporation of Al induced during the laser–material interactions that give rise to melting of the material.

The amount of aluminum loss is proportional to the temperature of the melt pool and the duration of the melting/re-solidifying process. This affects the redistribution of second-phase impurities and the precipitation of new phases. It also can lead to zone refinement of the melt at the top of the ridges, driving the impurities towards the bottom of the grooves where the last melt solidifies.

When the surface was inspected via SEM, it was revealed that there were regularly spaced molten pockets in the circumferentially grooved specimen [Fig. 5(d)]. Upon examination it was revealed that these corresponded to regions where the laser passed over twice during the microgrooving process.

The alumina-blasted surface showed a larger percentage of Al present at the surface than is expected (i.e., >6%). This most likely was the result of alumina having been embedded in the surface of the implant (Fig. 7). This not only changes the material structure of the implant, but it also raises the cytotoxicity as Al is known to be cytotoxic.[7,44] Large regions of the surface had large pockets of Al embedded deeply (Fig. 4). To understand how this affects cells, long-term cytotox-

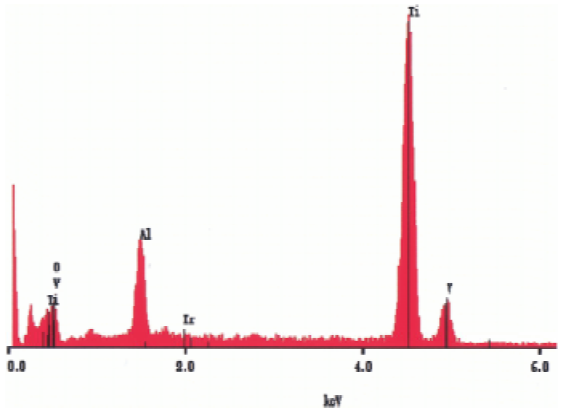

Figure 7. EDS spectrum of an Al_2O_3-blasted surface. Note the high Al peak. [Color figure can be viewed in the online issue, which is available at www.interscience.wiley.com.]

icity experiments must be performed and the dynamic changes in both the cell and the substrate monitored.

The polished surface was not appreciably changed from the bulk as polishing is a less aggressive treatment (than alumina blasting and laser texturing), thus causing less of a change in the surface structure and microchemistry.

The above changes in surface microchemistry associated with the different surface-texturing methods are important for three reasons. First, they may give rise to the enhancement of the local concentration of cytotoxic elements such as Al and V.[7,44] Such cytotoxic elements may explain, in part, the differences in results obtained from prior studies of the effects of laser texturing on cell–surface interactions with Ti/Ti-6Al-4V.[9–11,22–27] Second, the variations in surface chemistry affect the local surface energies and ultimately result in large variations in cell adhesion/integration. Third, the variations in cell surface chemistry result in differences in the structural/mechanical integrity of textured Ti6Al4V implants.

In the case of the textured Ti-6-Al-4V surfaces examined in this study, the variations in composition across the surfaces and cross sections were studied using semi-quantitative energy dispersive X-ray spectroscopy (EDS). The measured ranges in surface chemistry are presented in Table I. Elemental maps of the surface regions also are presented in Figures 6 and 7. These show the respective spatial distributions of Al and V in the different textured surfaces. The local variations in the chemical compositions of these elements could give rise to cytotoxic reactions that are sensitive to laser-processing conditions.

Cell–surface interactions

Cell morphology was examined using SEM operated at 5 kV. The cells growing on the microgrooved surfaces were observed to follow the direction of the grooves (contact guidance) and thus had some organization (Figs. 8 and 9). The cells on the alumina-blasted surface showed no organization and spread in a random fashion [Fig. 10(a,b)].

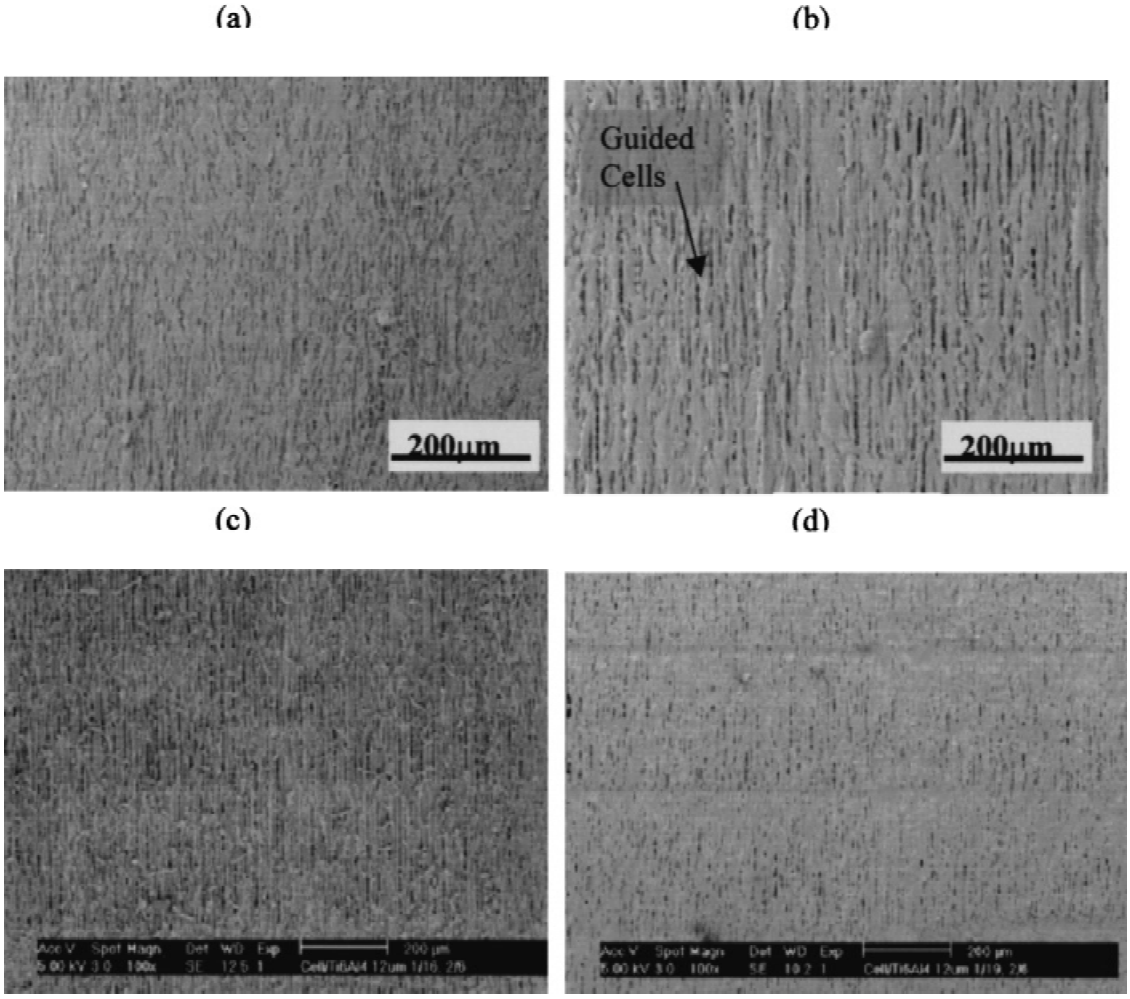

Figure 8. Cells growing on 12-μm grooves after (a) 1 day; (b) 2 days; (c) 5 days; and (d) 9 days.

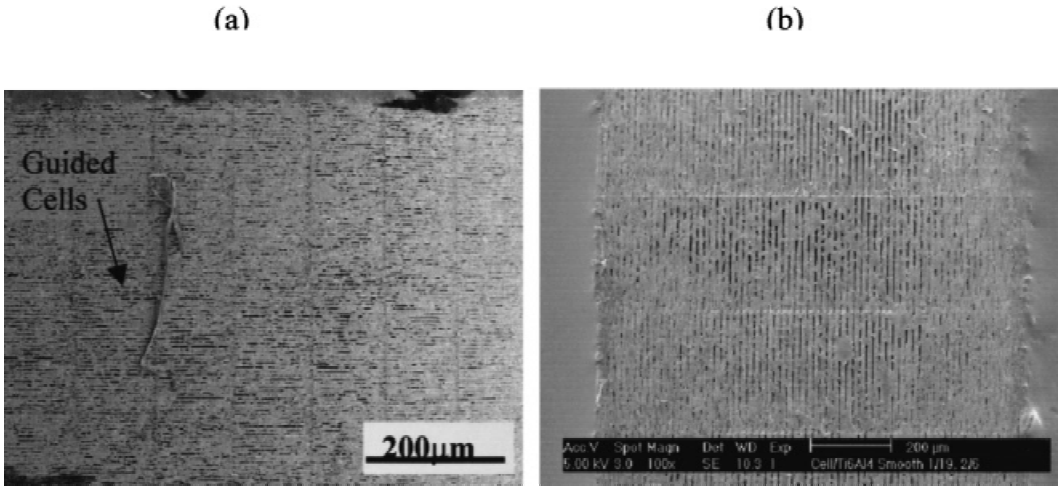

Figure 9. Cells growing on 8-μm grooves after (a) 2 days and (b) 9 days.

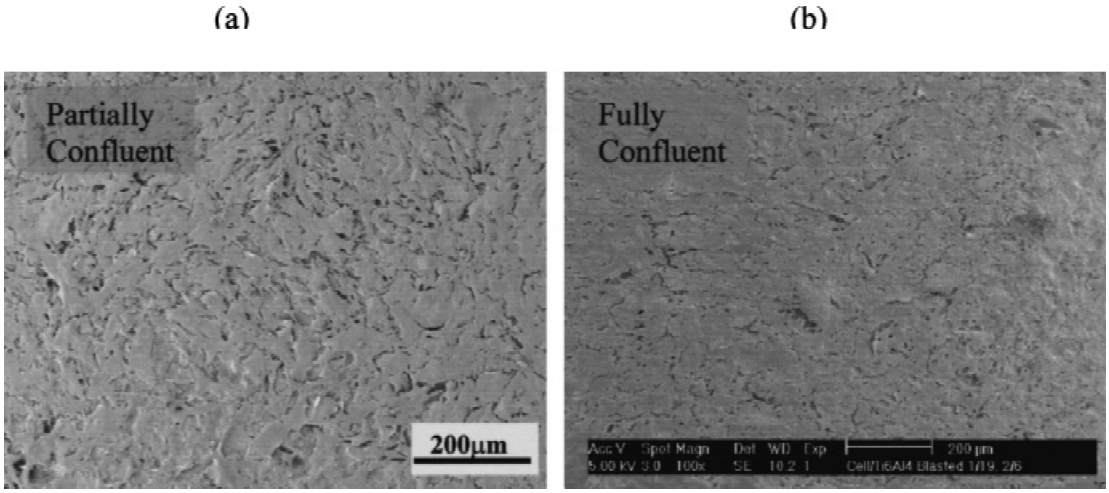

Figure 10. Cells growing on alumina-blasted surfaces after (a) 2 days and (b) 9 days.

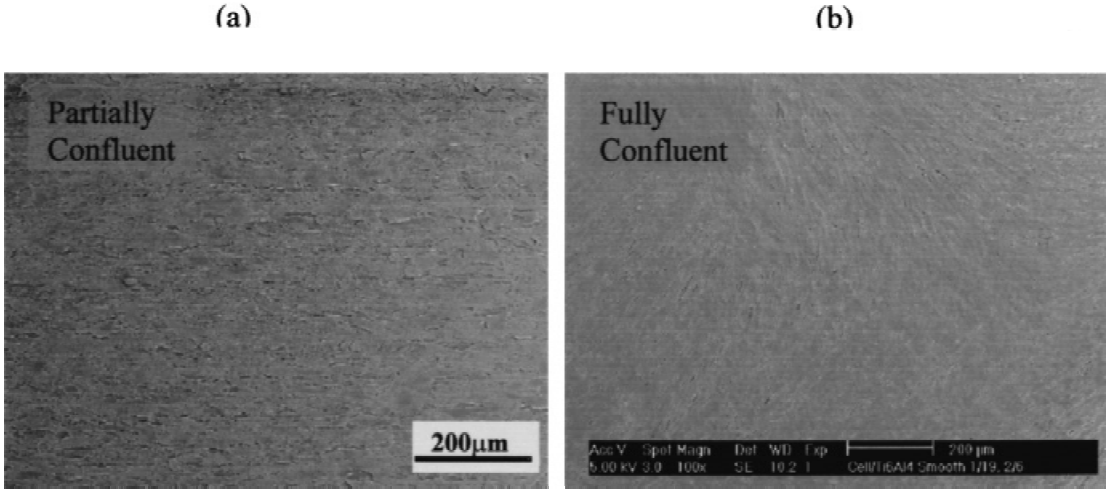

Figure 11. Cells growing on polished surfaces after (a) 2 days and (b) 9 days.

The cells on the smooth surface were somewhat organized, but not to the extent that the cells growing on the grooved surface were [Fig. 11(a,b)]. This should not be true for the smooth samples as there should be no features on the smooth surface to promote contact guidance. However, as shown earlier in the AFM and SEM analyses, the polishing process itself introduced small grooves at the submicron level [Figs. 2(a) and 9]. These most probably were the grooves that promoted the observed contact guidance on the polished surfaces.

In the latter stages of cell growth, cells, with flatter surfaces, were seen to be spreading, and there were fewer filopodia observed in the cell membrane. These filopodia are a storage area for extra cell membrane.[3] Hence, as the cells attach to the surfaces, the excess membrane is used up in the spreading process (Fig. 12). The filaments seen after 2 days have totally vanished after 9 days, implying a more complete spreading of the cells [Fig. 12(a,b)].

By the 2nd day, the cells already had begun to produce extra-cellular matrix on all four surfaces (Fig. 13) as well as having formed a noticeable number of attachments between cells (Fig. 9). This eventually lead to complete confluence, where the surface was covered by a continuous sheet of cells (Fig. 13). The extracellular matrix formation was more noticeable on the textured surfaces, especially on the grooved surfaces, compared to the smooth surfaces. Even by day 2 the cells growing on the grooved surfaces had developed a certain amount of extra-cellular matrix, tying the individual cells together, while the sandblasted surface had less, and the smooth surface even less [Fig. 13(a–d)]. This could partly explain why scar-tissue formation and fibrous encapsulation of smooth implants occurs during *in vivo* studies.[3]

By the 9th day, all the surfaces had extra-cellular matrix formation [Fig. 13(a–d)] and confluence had been reached, except for small regions on the grooved surfaces. Also, by the 9th day the cells on the grooved surfaces had fully aligned within the grooves and had formed a well-organized structure. In all cases, only a single layer of cells was observed for cell culture durations up to 9 days. Also, similar cell–surface phenomena were observed in the longitudinal and circumferential laser microgrooved geometries [Fig. 1(a–c)].

Finally, in this section the effects of surface topography on cell orientation are illustrated in Figure 14(a–d), in which histograms of cell orientation are presented for the four surfaces after 9 days of cell culture. Random cell orientations are observed on the blasted and smooth surfaces, as shown in Figures 10(b) and 11(b), respectively. Such random cell orientations may lead to increased scar-tissue formation during wound healing.[8] In contrast, clear evidence of contact guidance is observed on the surfaces of the 8- and 12-μm microgrooved geometries [Figs. 8(b) and 9(d)], giving rise to the narrow range of cell orientations that are close to the microgroove orientations.

Implications for tissue engineering

The current work suggests that 8–12-μm microgrooves can be used to promote contact guidance of osteoblasts on Ti6Al4V surfaces. Such aligned osteoblasts could give rise to reduced scar-tissue formation while promoting improved cell integration and adhesion.[3,4] However, the resulting adhesion will be directional in nature. Multidirectional groove designs therefore may be needed for the design of improved adhesion in different directions. Further work is

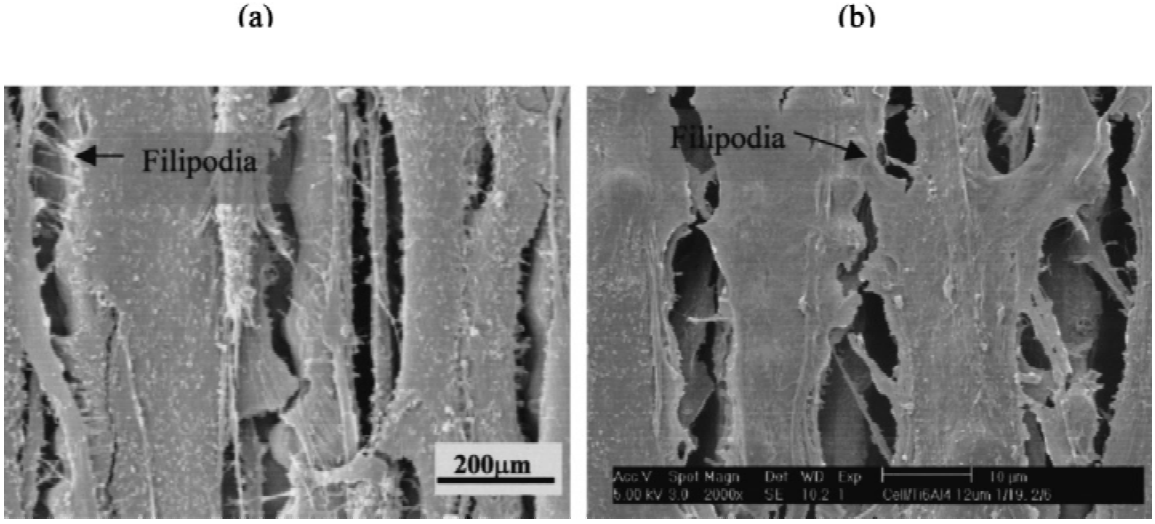

Figure 12. Cells attaching to 12-μm surfaces after (a) 2 days and (b) 9 days.

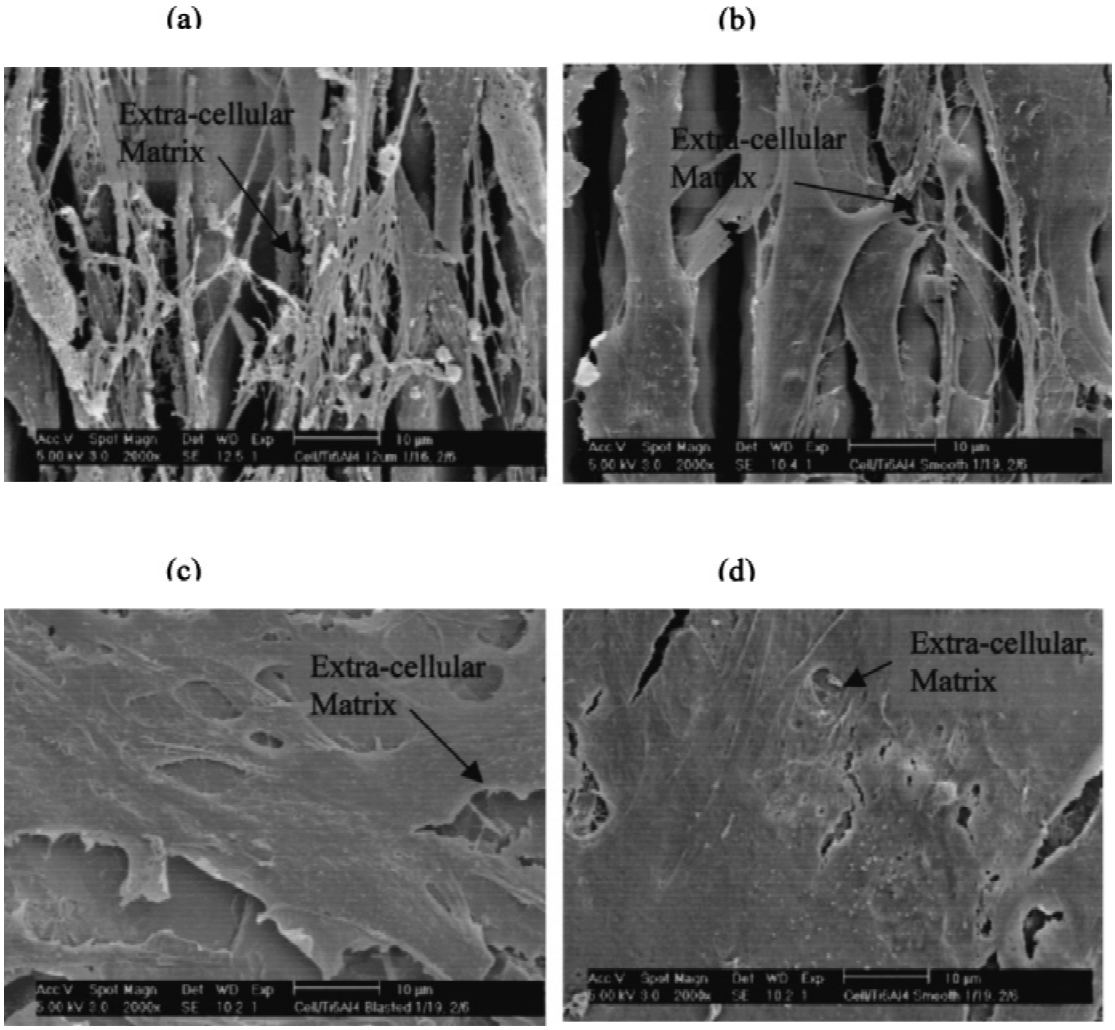

Figure 13. Extracellular matrix formation after 9 days of cell culture on (a) 12-μm microgrooved substrate; (b) 8-μm microgrooved substrate; (c) Al_2O_3-blasted surfaces; and (d) smooth surfaces.

needed to optimize the microgroove designs. This may involve the use of laser microgrids that promote contact guidance across different directions. Circumferential contact guidance across cylindrical cross sections also should be explored for Ti6Al4V hip and dental implants.[2]

Current Ti6Al4V implants result only in ~20% integration with bone.[5,35,36] However, there are no existing applications of laser microgrooved Ti6Al4V surfaces although some microgroove geometries are undergoing clinical trials.[3] Instead, existing Ti6Al4V hip implants rely on the use of roughened or porous surfaces, or surfaces with macrotextures and macroporosity (on the order of millimeters). The roughened surfaces and macrotextures promote improved cell–surface integration while porous hydroxyapatite surfaces promote biologic fixation.[37] However, such surfaces result in random cell alignment that can give rise to scar-tissue formation.[8] It also is unlikely that significant improvements in cell–surface integration can be achieved just by the incremental modification of macrotexture or macroporosity.

In contrast, the laser microgrooved surfaces offer an alternative approach to the engineering of improved cell–surface integration that is yet to be fully exploited in applications. This is in spite of the significant amount of prior research work[3,4] that has been done on laser-textured Ti-6Al4V surfaces.

Furthermore, in addition to promoting contact guidance and improved integration with bone cells and soft tissue in *in vivo* canine experiments,[4] the restricted cell spreading on the surfaces provides enough room for the combined integration of soft tissue and bone cells in dental implants. Such combined integration is critical to the long-term performance of Ti6Al4V implants in dental applications.[3,4]

Before concluding, it is important to discuss some of the possible differences between the 8–12-μm microgrooves and the much smaller microgroove geometries that have been used in prior studies of cell–

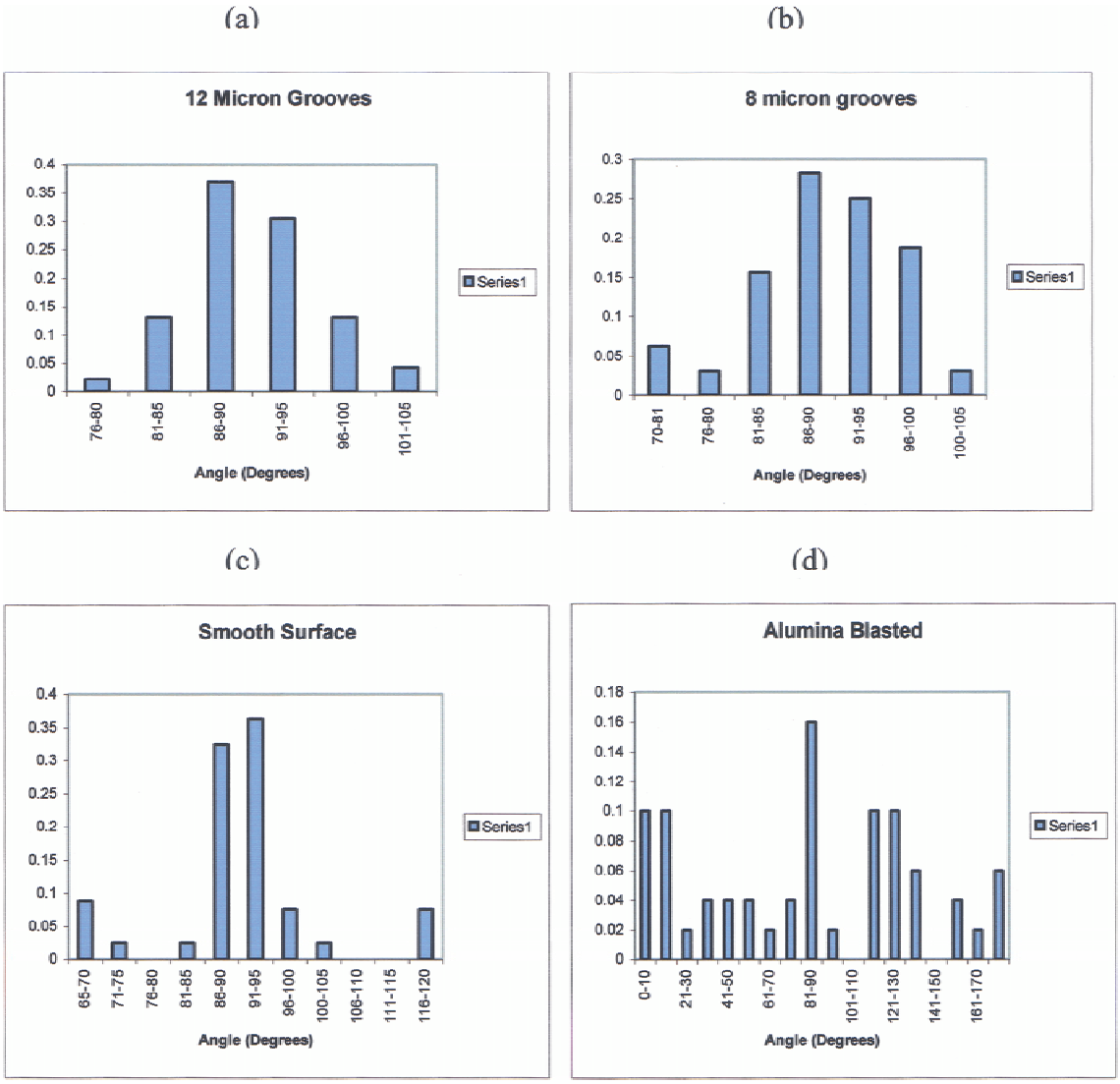

Figure 14. Histograms showing variations in cell orientations after 9 days of cell culture on (a) 12-μm microgrooved substrate; (b) 8-μm microgrooved substrate; (c) smooth surfaces; and (d) Al_2O_3-blasted surfaces.

surface interactions by Walboomers et al.[36] These studies[36] have used smaller (~1 μm) microgroove geometries instead of the 8–12-μm laser-microgrooved geometries that were used in the current study. It was suggested that larger microgrooves (greater than ~1 μm in depth) can result in increase plaque uptake in dental applications. However, the smaller microgrooved geometries were not observed to exhibit contact guidance, as was observed in the 8–12-μm grooves used in the current study. The differences may be attributed partly to local differences in microchemistry (Figs. 6 and 7) as well as to local differences in microgroove geometry.[45]

In contrast, similar observations of cells (spreading over smaller 2-μm grooves and contact guidance along 12-μm microgrooves) have been reported on microgrooved polystyrene culture plates produced using semiconductor fabrication techniques.[4] Prior work by Ohara and Buck[46] also has shown that cells can align with fine grooves produced by polishing while the laser implant surfaces have been studied by Kasemo and Gold.[47] However, this is the first report (that the authors are aware of) of contact guidance on 8–12-μm laser-microgrooved Ti6Al4V surfaces.

Finally, it is important to discuss the implications of the observations of "smooth" and roughened surfaces that are used in existing Ti6Al4V implants. Such surfaces give rise to random cell orientations that are likely to result in increased scar tissue formation.[4,8] However, the interfacial properties are likely to be more isotropic than those between laser microgrooved surfaces and bone cells/soft tissue. Clearly, further work is needed to determine the anisotropy in cell–surface adhesion for the Ti6Al4V surfaces examined in this study. Research also is needed to explore the effects of interfacial geometry/microstructure on inter-

facial strength,[48,49] fatigue resistance,[50] and intracellular communication.[51,52]

CONCLUSIONS

The interactions between MC3T3-E1 osteoblasts and textured surfaces have been studied along with the differences in surface topography, surface and bulk microstructure, and surface microchemistry produced by laser microgrooving, alumina blasting, and polishing. The following conclusions have been reached from the multiscale characterization of Ti6Al4V surfaces and cell–surface interactions:

1. At the nanoscale, the surfaces exhibit representative surface topographical features that are well characterized by AFM RMS values. The laser-textured surfaces are rougher (RMS roughness of ~70–117 nm) than the Al_2O_3-blasted surfaces (44 nm), which are rougher than the polished surfaces (32 nm). The RMS values increase with decreasing fractal dimensions. However, the relatively small changes in the fractal number (2.6–2.10) suggest that the surface complexity is not significantly affected by the different surface texturing schemes.
2. The nanoscale characterization also provides useful qualitative information on the effects of surface texturing. This includes evidence of nanoscale grooves for the Al_2O_3-blasted and polished surfaces. Such grooves may be used to pattern nanoscale geometrical features onto the surfaces of biomedical implants. However, the effects of surface texturing on microgroove dimensions must be established through a careful series of well-controlled experiments. The nanoscale grooves also may provide a template for subsequent interactions of synthetic biomedical surfaces with protein molecules.
3. At the submicron scale (between the nano- and microscale), TEM analysis of the laser-textured surfaces revealed a layered, re-solidified microstructure consisting predominantly of a hexagonal, closed, packed α phase, this in spite of the depletion in Al content (α stabilizer) that occurs in the surface regions during laser processing. Some contamination of the grooves with Mo, Cr, and other elements also was observed at the bottom of the grooves. The source of these contaminants is yet to be established. Since Mo and Cr are β stabilizers in α/β titanium alloys, they should stabilize the β phase. Nevertheless, the electron diffraction analysis of the bottom of the grooves revealed only the presence of the α phase. This suggests that the observed structures produced via laser processing may be metastable.
4. The microscale analysis of the laser-textured surfaces revealed a complex, re-solidified microstructure that is somewhat analogous to that of laser welded α/β titanium alloys. This includes a re-solidified region with "Chinese script" precipitates and dendritic morphologies. A complex solidification cracking morphology also was observed in the re-solidified region, with cracks that were ~5 μm long. The cracks terminated at the boundary between the re-solidified zone and the heat-affected zone. However, they may contribute to subsequent fatigue-induced damage in subsequent biomedical applications. Therefore attempts should be made to eliminate, or reduce, the extent of cracking by the control of laser process variables.
5. The SEM (microscale) analysis also revealed the presence of regularly spaced molten pockets that correspond to the regions that were heated twice during laser processing. These were observed only in the circumferential laser-textured specimens, presumably as a result of the double exposure of these regions to laser ablation. Since the structures of the re-solidified molten pockets may degrade performance, attempts should be made to minimize the double exposure of the textured materials during laser ablation.
6. The 8–12-μm microgroove geometries promote contact guidance along a narrow range of angles. In contrast, the smooth and alumina-blasted roughened surfaces promote random cell orientations that are likely to give rise to increased scar-tissue formation. In general, however, the alumina-blasted and the 8- and 12-μm microgrooved geometries result in restricted cell spreading compared to smooth Ti6Al4V surfaces. The extent of cell spreading also appears to decrease with increased surface roughness.

Appreciation is extended to Professors Jeremiah Ostryker, Anthony Evans, Alexander Smits, Van Thompson, and Dianne Rekow for their encouragement and support. The authors also are grateful to Ms. Elizabeth Clark and Mr. Chris Arena for their assistance with the cell culture experiments. Finally, the authors thank Professor Barrie Royce for stimulating discussions on cell–surface interactions.

References

1. Dobbs HS, Scales JT. Behavior of commercially pure titanium and Ti6Al4V orthopaedic implants. In: Lucki HA, Kubli F, editors. STP 796. Philadelphia: American Society for Testing and Materials; 1983. p 174.
2. Rattner B, Hoffman A, Schoen F, Lemons J. Biomaterials sci-

ence: An introduction to materials in medicine. New York: Academic Press; 1996.
3. Ricci JL, Charvet J, Frenkel SR, Chang R, Nadkarni P, Turner J, Alexander H. Bone engineering. In: Davies JE, editor. Bone response to laser microtextured surfaces. Toronto: Em^2 Inc.; 2000. p 1–11.
4. Ricci JL, Spivak JM, Blumenthal NC, Alexander H. Modulation of bone ingrowth by surface chemistry and roughness. In: Davies JE, editor. The bone–biomaterial interface. University of Toronto Press; 1991. p 334–349.
5. Bauer G. Biochemical aspects of osseointegration. In: Heimke G, editor. Osseointegrated implants: Basics, materials, and joint replacement. Boca Raton, FL: CRC Press; 1990.
6. Cales B, Blaise L, Stefanie Y. Medical uses of zirconia [review]. Minneapolis: Society of Biomaterials, Symposium E; 2000.
7. Anselme K, Noel B, Hardouin P. Human osteoblast adhesion to titanium alloy, stainless steel, glass and plastic substrates with the same surface topography. Mater Med 1999;10:815–819.
8. Wang JH-C, Grood ES, Florer J, Wenstrup R. Alignment and proliferation of MC3T3-E1 osteoblasts in microgrooved silicone substrate subjected to cyclic stretching. J Biomech 2000;33: 729–735.
9. Brunette DM, Chehroudi B. The effects of surface topography of micromachined titanium substrata on cell behavior *in vitro* and *in vivo*. J Biomech Eng 1999;121:49–57.
10. Brunette DM. Fibroblasts on micromachined substrata orient hierarchically to grooves of different dimensions. Exp Cell Res 1986;164:11–26.
11. den Braber ET, Jansen HV, de Boer MJ, Croes HJE, Elwensproek M, Ginsel LA, Jansen JA. Scanning electron microscopic, transmission electron microscopic, and confocal laser scanning microscopic observation of fibroblast cultures on microgrooved surfaces of bulk titanium substrate. J Biomed Mater Res 1998;40:425–433.
12. Hakura Y, Kosugi A, Sudo H, Yamamoto S. Development of new system for evaluating the biocompatibility of implant materials using an osteogenic cell line (MC3T3-E1). J Biomed Mater Res 1988;20:613–622.
13. Wieland M, Textor M, Spenser ND, Brunette DM. Wavelength-dependent roughness: A quantitative approach to characterizing the topography of rough titanium surfaces. Int J Oral Maxillofac Impl 2001;16:163–181.
14. Mandelbrot BB. The fractal geometry of nature. San Francisco: Freeman; 1982.
15. Underwood EE, Banerji K. Metals handbook. Vol. XII. Fractography. 9th ed. Materials Park, OH: American Society for Metals; 1987. p 211.
16. Baeslack WA III, Chiang S, Albright CA. Laser welding of an advanced rapidly solidified titanium alloy. J Mater Sci 1990;21: 698–702.
17. Collings EW. The physical metallurgy of titanium alloys. Metals Park, OH: American Society for Metals; 1984.
18. Reed-Hill R, Abbaschian R. Physical metallurgy principles. Boston: PWS Publishing Company; 1994.
19. Courtney TH. Mechanical behavior of materials. New York: McGraw-Hill; 1990.
20. von Recum AF, Shannon CE, Cannon EC, Long KJ, van Kooten TG, Meyle J. Surface roughness, porosity, and texture as modifiers of cellular adhesion. Tissue Eng 1996;2:241–253.
21. Brunette DM. Effects of surface topography on cell behavior *in vitro* and *in vivo*. In: Hoch HC, editor. Nanofabrication and biosystems. New York: Cambridge University Press; 1996. p 335–366.
22. Inoue T, Cox JE, Piliar RM, Melcerh AH. Effect of the surface geometry of smooth and porous-coated titanium alloy on the orientation of fibroblasts *in vitro*. J Biomed Mater Res 1987;21: 107–126.
23. Chehroudi B, Gould TRL, Brunette DM. Effects of a grooved titanium-coated implant surface on epithelial cell behavior *in vitro* and *in vivo*. J Biomed Res 1990;24:1067–1085.
24. Brunette DM, Kenner GS, Gould TRL. Grooved titanium surfaces orient growth and migration of cells from human gingival explants. J Dent Res 1983;62:1045–1048.
25. Chehroudi B, Gould TRL, Brunette DM. Effects of a groove titanium-coated implant surface on epithelial cell behavior *in vitro* and *in vivo*. J Biomed Mater Res 1989;23:1067–1085.
26. Walboomers XF, Croes HJE, Ginsel LA, Jansen JA. Growth behavior of fibroblasts on microgrooved polystyrene. Biomaterials 1998;19:1861–1868.
27. Chesmel K, Black J. Cellular responses to chemical and morphologic aspects of biomaterial surfaces. I. A novel *in vitro* model system. J Biomed Mater Res 1995;29:1089–1099.
28. Meyle J, Gultig K, Nisch W. Variation in contact guidance by human cells on a microstructured surface. J Biomed Mater Res 1995;29:81–88.
29. von Recum AF, van Kooten TG. The influence of microtopography on cellular response and the implications for silicone implants. J Biomater Sci, Polym Edn 1995;7:181–198.
30. Curtis ASG, Wilkinson C. Topographical control of cells. Biomaterials 1997;18:1573–1583.
31. Weiss P. Experiments on cell and axon orientation *in vitro*: The role of colloidal exudates in tissue organization. J Exp Zool 1945;100:353–386.
32. Britland S, Morgan H, Wojiak-Stodart B, Riehle M, Curtis A, Wilkinson C. Synergistic and hierarchical adhesive and topographic guidance of BHK cells. Exp Cell Res 1996;228:313–325.
33. Clark P, Connoly P, Curtis ASG, Dow JAT, Wilkinson CDW. Topographical control of cell behaviour. J Simple Step Clues Dev 1987;99:439–448.
34. Ohara PT, Buck RC. Contact guidance *in vitro*. A light, transmission and scanning electron microscopic study. Exp Cell Res 1979;121:235–249.
35. Meyle J, Gutig K, Wolburg H, von Recum AF. Fibroblast anchorage to microtextured surfaces. J Biomed Mater Res 1993; 27:1553–1557.
36. Walboomers XF, Croes HJE, Ginsel LA, Janson JA. Contact guidance of rat fibroblasts on various implant materials. J Biomed Mater Res 1999;47:204–212.
37. Puleo DA, Nanci A. Understanding and controlling the bone–implant interface. Biomaterials 1999;20:2311–2321.
38. von Recum AF. Applications and failure modes of percutaneous devices: A review. J Biomed Mater Res 1984;18:323–336.
39. Clark P, Connolly P, Curtis ASG, Dow JAT, Wilkinson CDW. Topographical control of cell behavior. II. Multiple grooved substrata. Development (Cambridge, UK) 1990;108:635–644.
40. Ito Y. Surface micropatterning to regulate cell functions. Biomaterials 1999;20:2333–2342.
41. Kam L, Shain W, Turner JN, Bizios R. Correlation of astroglial cell function on micro-patterned surfaces with specific geometric parameters. Biomaterials 1999;20:2343–2350.
42. Lu L, Kam L, Hasenbein M, Nyalakonda K, Bizios R, Gopferich A, Young JF, Mikos AG. Retinal pigment epithelial cell function on substrates with chemically micropatterned surfaces. Biomaterials 1999;20:2351–2361.
43. Kane RS, Takayama S, Ostuni E, Ingber DE, Whitesides GM. Patterning proteins and cells using soft lithography. Biomaterials 1999;20:2353–2376.
44. Anselme K, Linez P, Bigerelle M, Le Maguer D, Le Maguer A, Hardouin P, Hildebrand HF, Iost A, Leroy JM. The relative influence of the topography and chemistry of Ti6Al4V surfaces on osteoblastic cell behaviour. Biomaterials 2000;21:1567–1577.
45. Soboyejo WO, Mercer C, Allameh S, Nemetski B, Marcantonio N, Ricci JL. Multi-scale microstructural characterization of mi-

cro-textured Ti-6Al-4V surfaces. In: Katsube N, Soboyejo WO, Sacks M, editors. Functional biomaterials. Switzerland: Trans Tech Publications; 2001. p 203–227.
46. Ohara PT, Buck RC. Contact guidance *in vitro*: A light transmission and scanning electron microscopy. Exp Cell Res 1979; 121:235–249.
47. Kasemo B, Gold J. Implant surfaces and interface processes. Adv Dent Res 1999;13:8.
48. Haddad RJ Jr., Cook SD, Thomas KA. Biological fixation of porous coated implants. J Bone Joint Surg 1987;69A:1459–1466.
49. Thomas KA, Kay JF, Cook SD, Jarcho M. The effect of surface texture on the mechanical strengths and histologic profiles of titanium implant materials. J Biomed Mater Res 1987;21:1395–1414.
50. Wolfarth B, Ducheyne P. Effect of change in interfacial geometry on the fatigue strength of porous-coated Ti6Al4V. J Biomed Mater Res 1994;28:417–442.
51. Tuan RS. Cellular and molecular events during bone–implant interaction. Scripta Metallurgica Mater 1994;31:971–976.
52. Shah AK, Lazatin J, Sinha RK, Lennox T, Hickok NJ, Tuan RS. Mechanism of BMP-2 stimulated adhesion of osteoblastic cells to titanium alloy. Biol Cell 1999;91:131–142.